Stick-slip motion of surface point defects prompted by magnetically controlled colloidal-particle dynamics in nematic liquid crystals

Michael C. M. Varney,[1] Qiaoxuan Zhang,[1,2] and Ivan I. Smalyukh[1,2,3,4,*]

[1]*Department of Physics, University of Colorado at Boulder, Boulder, Colorado 80309, USA*

[2]*Materials Science and Engineering Program, University of Colorado at Boulder, Boulder, Colorado 80309, USA*

[3]*Department of Electrical, Computer, and Energy Engineering and Soft Materials Research Center,*
University of Colorado at Boulder, Boulder, Colorado 80309, USA

[4]*Renewable and Sustainable Energy Institute, National Renewable Energy Laboratory*
and University of Colorado at Boulder, Boulder, Colorado 80309, USA

We explore the dynamics of topological point defects on surfaces of magnetically responsive colloidal microspheres in a uniformly aligned nematic liquid crystal host. We show that pinning of the liquid crystal director to a particle surface with random nanostructured morphology results in unexpected translational dynamics of both particles and topological point defects on their surfaces when subjected to rotating magnetic fields. We characterize and quantify the "stick-slip" motion of defects as a function of field rotation rates as well as temperature, demonstrating the roles played by the competition of elastic forces, surface anchoring, and magnetic torques on the sphere as well as random-surface-mediated pinning of the easy axis of the nematic director on colloidal microspheres. We analyze our findings through their comparison to similar dynamic processes in other branches of science.

PACS number(s): 61.30.−v

I. INTRODUCTION

Solid friction behavior, specifically stick-slip motion [1–8], describes a wide range of physical phenomena encountered in daily life. It describes the squeaking of chalk on a chalkboard and the squeaking of sand compressed underfoot on a beach [2], as well as low-frequency rumblings of a fault shift during earthquakes [3]. In acoustics it explains the stridulation (chirping) of crickets and the spiny lobster [4] and the beautiful sound of bowed instruments, such as the cello [5]. Studies of defect motion also span many branches of modern science and technology [9–22]. For example, dynamics of dislocations permits metals to be plastically deformable with ease, a circumstance upon which our modern technology is highly dependent [9,10]. Dynamics of cosmic strings, topological defect lines that might have governed early universe development, may be modeled by considering nematic disclinations emerging during the isotropic-nematic phase transition [10–13]. In various liquid crystal (LC) phases, defects often determine the physics and dynamics of numerous irreversible phenomena, such as when a liquid crystal reacts to an applied electric and magnetic fields, flow, or anchoring-transition-mediated changes of boundary conditions [14–19]. Controlling dynamics of creation and annihilation of defects in certain LC display modes is important to avoid degraded performance [19]. In solid-state physics, glide and climb of dislocations are associated with a broad range of interesting fundamental phenomena, such as Peierls-Nabarro friction [9,17]. In this case, as the dislocation glides across a periodic crystal lattice, the defect core structure changes accordingly, so atomic reconstructions lead to periodic changes in the potential energy of the crystal. The applied stress needed to overcome the ensuing energy barriers is called the Peierls-Nabarro stress and is determined by the core

structure of corresponding defects [9]. Solid friction behavior, including the stick-slip motion, was previously described for several classes of line and wall defects in different condensed matter systems, examples of which include domain walls in thin magnetic films [20], π-wall defects in LCs [21], and vortices in superconductors [22].

In this work, we design and implement an experimental soft matter system to explore stick-slip dynamics of surface point defects dubbed "boojums" [23–26]. Superparamagnetic beads (SPMB) [26] with rough morphology and characteristic random surface features on the scale of 50–100 nm are incorporated into a nematic LC (NLC) host with an aligned far-field director $\mathbf{n_0}$ [14,27]. Complex interactions of the LC with these colloidal surfaces result in nondegenerate surface anchoring [28] of the LC director $\mathbf{n}$ and a "memorized" $\mathbf{n(r)}$ director field configuration with two boojums at the particle's opposing poles along $\mathbf{n_0}$. When these colloidal SPMBs are rotated by in-plane ac magnetic fields, induced magnetic torques on the particle compete with surface anchoring and elastic torques resulting from nondegenerate tangential surface anchoring of $\mathbf{n(r)}$ on the particle surface and ensuing particle-induced elastic distortions in the LC bulk. This induces unexpected and complex motions of both the colloidal particles and the topological point defects (boojums) on their surfaces. We identify and characterize this fascinating and previously unreported boojum stick-slip motion, as well as compare it to similar phenomena in diverse physical systems.

II. MATERIALS, METHODS, AND TECHNIQUES

A. Holonomic magnetic and holographic optical manipulation system

Magnetic and optical manipulation of magnetically responsive colloids is achieved by combining holographic optical trapping (HOT) with a three-axis electromagnetic apparatus formed by solenoids (S52051, from Fisher Scientific

---

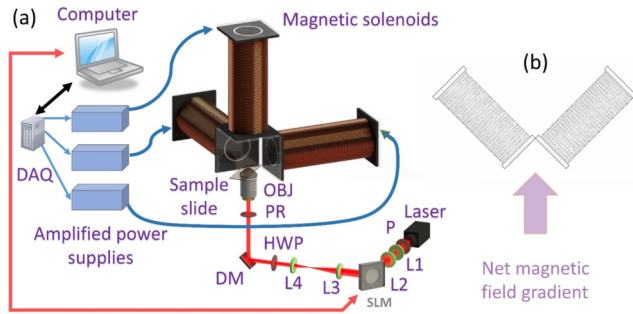*Corresponding author: ivan.smalyukh@colorado.edu

FIG. 1. (Color online) Integrated holonomic magnetic and holographic optical manipulation system. (a) Electromagnetic solenoids arranged on a Cartesian aluminum frame mounted on an inverted microscope (not shown). The solenoids are driven by amplified power supplies via computer-controlled DAQ. The HOT is based on a fiber laser and an optical setup with the following optical elements: polarizer (P), lenses of two telescopes (L1, L2, L3, L4), computer-controlled, dynamically addressable liquid crystal based spatial light modulator (SLM), a $100\times$ oil immersion objective (OBJ), half-wave plate (HWP), polarization rotator (PR), and a dichroic mirror (DM). The trapping beam is focused within the sample volume. This manipulation setup is integrated with an optical imaging system capable of both POM and 3PEF-PM imaging. (b) Two solenoids arranged in the x-y plane aligned with the microscope's focal plane. The direction of the net magnetic force due to magnetic field gradients in this configuration is shown by the arrow.

International, Inc.) [26]. The solenoids contain custom-machined cast-iron cores and are arranged on an aluminum Cartesian frame mounted directly onto the microscope body [26]. Each electromagnet (Fig. 1) is independently driven via an amplified power supply (APS, model no. BOP20-5M, from Kepco), which is controlled using a computer-driven data acquisition card (DAQ, model no. USB-6259 BNC, from National Instruments) via our in-house LABVIEW-based software (LABVIEW was obtained from National Instruments). These electromagnets can produce ac and/or dc magnetic fields up to a maximum of about 108 G at magnetic field rotation rates of up to 8 Hz (typically much lower rotation rates were used in the present study), which enables manipulation of all magnetically responsive colloids in a sample simultaneously rather than controlling single colloids on an individual basis [26,28]. These low magnetic fields are found to have no significant direct coupling with the NLC director since most known LCs (including the ones used in this study) are diamagnetic materials, with the director realignment typically being a thresholdlike effect requiring fields of the order of 1000 G and higher.

Although the used solenoids are designed to minimize magnetic gradient forces within the sample volume, their cores have a finite radius and geometric arrangement which results in a residual in-plane fringe field gradient which can yield residual forces of up to 0.07 pN acting on our magnetically responsive colloids [Fig. 1(b)]. This gradient force is directed along the y axis (in a two solenoid configuration), as shown by an arrow in Fig. 1(b) [26]. Although this gradient force is relatively weak, comparable to the gravity forces acting on particles within our colloidal suspension, it slowly translates the colloidal particles while being balanced by a viscous drag

in the host medium. This motion results in significant particle displacements over extended time periods, which must be accounted for experimentally.

Optical microscopy observations were performed using an inverted polarizing optical microscope (POM) (Olympus IX81) with a $100\times$ or $60\times$ oil immersion objective of numerical aperture ≈ 1.4. Optical video microscopy was used to probe colloidal particle and defect dynamics through recording their motion with a charge-coupled-device camera (Flea, PointGrey) or a slow-motion camera (HotShot 512SC, from NAC Image Technology, Inc.) and then determining their time-dependent spatial positions from captured image sequences using motion tracking software (IMAGEJ, obtained from the National Institute of Health). The time-dependent coordinates describing the boojum and particle positions relative to stationary or moving reference frames [26] are then used to characterize rotational and translational motions induced by a rotating magnetic field, as reported in detail below. Optical manipulation and assembly of SPMB dimers were realized with a holographic optical tweezers setup operating at a wavelength of 1064 nm and integrated with the same optical microscopy system [26]. The temperature of LC colloidal samples was controlled via an objective heater (from Biological Optical Technologies, Inc.).

B. Sample preparation

We use a single-compound nematic LC pentyl-cyanobiphenyl (5CB, from Frinton Laboratories) with a nematic-isotropic phase transition temperature of $\approx 35\,°C$, in which we disperse magnetically responsive colloidal particles either via solvent exchange or through sedimentation mixing [26]. Sample cells are constructed from glass slide substrates cleaned in a water and detergent sonication bath at $60\,°C$; sequentially rinsed with acetone, methanol, and isopropylalcohol, and then dried and plasma cleaned. Planar alignment boundary conditions on the substrates are set using an anchoring layer. This alignment layer is prepared using polyvinyl alcohol (PVA) dissolved in deionized water at ≈ 1 wt. %. The aqueous PVA solution is spin coated at 8500 rpm and then baked at $100\,°C$ for at least 1 h. Rubbing this alignment layer with a velvet cloth forces the LC molecules to align along the rubbing direction and, thus, sets the planar surface boundary conditions for $\mathbf{n}(\mathbf{r})$. The resulting substrates are assembled into planar NLC cells by aligning their rubbing directions at confining surfaces facing each other in an antiparallel fashion, producing cells with a director pretilt angle within $3°$–$6°$ [26]. The cell gap thickness varying from 10 to 120 μm is set by interspacing the substrates with spherical silica spacers of corresponding diameters dispersed in a UV curable epoxy (NOA-61, from Norland Products) and interspacing glass plates sandwiched together. A colloidal dispersion of SPMBs in an NLC host was infused into the cells whose edges were then sealed with a fast setting epoxy.

The commercially available spherical magnetically responsive SPMBs (Dynabead M450, from Invitrogen) [26] are made of ferromagnetic nanoparticles (γ Fe_2O_3 and Fe_3O_4), which are approximately 8 nm in diameter, embedded into a highly cross-linked solid epoxy matrix at a density of $\sim 10^5$ nanoparticles per superparamagnetic bead (Fig. 2). Each
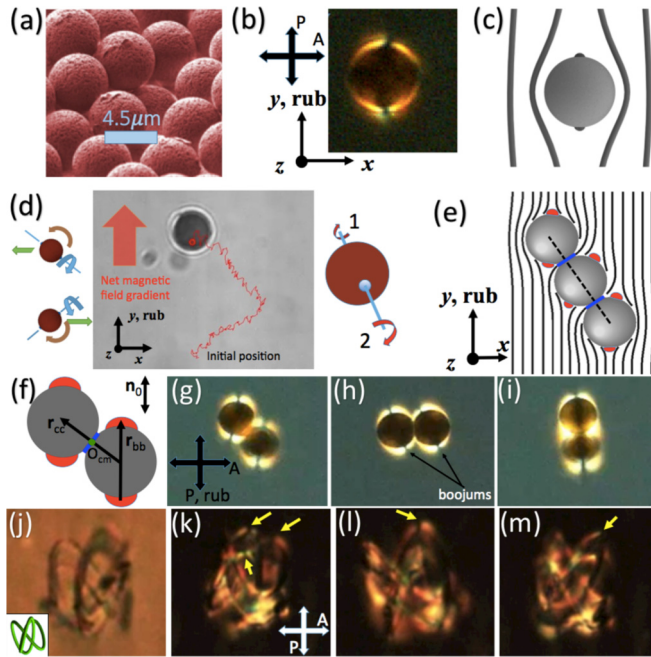
FIG. 2. (Color online) Superparamagnetic bead surface morphology, induced director structure, "walking" motion, and chain-dimer formation. (a) SEM image of a SPMB showing nanoscale surface roughness, which is responsible for a strong surface anchoring of the NLC director orientation at the surface determined to be tangential but with "memory" (nondegenerate); the color of the SEM image is artificial. (b) Polarizing optical micrograph obtained between crossed polarizers and (c) a schematic showing how the SPMB distorts the nematic director field, creating two surface point defects called "boojums," shown by hemispheres in (c) and seen as dark regions at the particle poles in (b). (d) Rotating an applied in-plane magnetic field **H** [brown (gray) CCW curved arrows on left] causes the SPMB to "barrel roll" out of the x-y plane [as shown using blue (gray) arrows on the left-side inset to the left from the optical micrograph], causing a "walking" motion of the SPMB along the x axis [green (gray) arrows on the left], while a constant net magnetic gradient force pulls the SPMB in the y direction. The "barrel-roll" motion is accompanied by a precession of one of the boojums around $\mathbf{n_0}$, while the other boojum circumscribes a smaller precessional arc. Switching the magnetic field rotation direction from clockwise to counterclockwise and vice versa reverses the direction of velocity component along the x axis. (e) A schematic of the director structure around an assembly of three SPMB particles with six $+1$ boojums in the director field at the NLC-particle interface [shown by red (dark gray) hemispheres] and side view of the neck regions marked by blue (gray) solid lines. (f) A schematic of a colloidal dimer defining its center of mass ($O_{c.m.}$), center-to-center separation vector between SPMBs ($\mathbf{r_{cc}}$) and boojum-to-boojum separation vector $\mathbf{r_{bb}}$ for one of the particles of the dimer. [(g)–(i)] Polarizing optical micrographs obtained between crossed polarizers as the dimer is manipulated magnetically and optically to orient $\mathbf{r_{cc}}$ away from the equilibrium orientation at no fields (g) to be, for example, orthogonal (h) or parallel (i) to $\mathbf{n_0}$. [(j)–(m)] Brightfield (j) and POM (k)–(m) micrographs showing magnetic rotation of a magnetically responsive microparticle shaped as a trefoil torus knot, with several of 12 induced boojums marked by yellow (gray) arrows. The images were extracted from the Supplemental movie S1 [29], which allows to see the defect-colloidal dynamics more clearly and in detail. The inset in (j) shows a schematic of the side view of a trefoil knot particle oriented with the torus plane

SPMB particle has a nominal diameter of $4.5 \pm 0.1\,\mu$m. When dispersed in an aligned liquid crystal and controlled by rotating external magnetic fields, individual SPMBs and their dimers, as well as larger assemblies, exhibit facile response to external magnetic fields (Supplemental movies S2 and S3 [29]). Additionally, trefoil-knot-shaped magnetically responsive microparticles are fabricated using two-photon photopolymerization and methodology described in detail elsewhere [30], but using a monomeric fluid doped with $CoFe_2O_4$ ferromagnetic nanoparticles with a mean diameter of 10 nm [31], so the ensuing complex-shaped superparamagnetic particles are responsive to external magnetic fields. These knot-shaped particles [Figs. 2(j)–2(m)] have the overall size of about 15 μm and the diameter of a cross section of the tube forming the knot being about 2 μm. These superparamagnetic colloidal knots are controlled by permanent magnets exerting fields of 200–400 G, as shown in the Supplemental movie S1 [29] and in Figs. 2(j)–2(m).

The ferrite nanoparticle orientations are mechanically coupled to the epoxy of the SPMB microsphere and therefore alignment of the net induced magnetic moment **m** forces the SPMB to point along and lock with the applied magnetic field **H**, as discussed in detail elsewhere [26],

$$\mathbf{m} = \mathbf{V_p}\chi_{\mathbf{p}}\mathbf{H},\tag{1}$$

with a resultant torque on the SPMB given by

$$\boldsymbol{\tau} = \mu\mathbf{m} \times \mathbf{H},\tag{2}$$

where V_p is the colloidal particle's volume, χ_p is its effective magnetic susceptibility, and μ is the colloid's magnetic permeability. We achieve magnetic torques of up to $\sim 5 \times 10^{-18}$ N m exerted on individual SPMBs [26].

III. RESULTS

A. SPMB-induced director structure and response to magnetic fields

Polarizing optical micrographs of SPMB particles dispersed in NLC cells, such as the one shown in Fig. 2(b), reveal that such particles induce tangential (planar) nondegenerate surface anchoring for $\mathbf{n}(\mathbf{r})$ of the surrounding NLC [26,28]. The director tends to pin to colloidal particle surfaces due to a phenomenon often referred to as the "anchoring memory." This behavior is consistent with the results of scanning electron microscopy (SEM) imaging of particle surfaces [Fig. 2(a)], which reveals nonuniform nanoscale surface morphology of a type that naturally allows for strong mechanical coupling between the surface of superparamagnetic beads, $\mathbf{n}(\mathbf{r})$, and surface-bound topological defects. Such coupling introduces a form of orientational mechanical friction between the SPMB surface and azimuthal orientation of $\mathbf{n}(\mathbf{r})$ tangential to its

---

FIG. 2. (*Continued*) orthogonal to $\mathbf{n_0}$ and with 12 boojums (not shown), which reside on the diametrically opposite sides of the knotted polymerized tube on the exterior and interior tip points of the knot along $\mathbf{n_0}$. Orientations of polarizer (P), rubbing direction (rub, defining orientation of $\mathbf{n_0}$), and analyzer (A) are marked by double arrows on the POM micrographs.
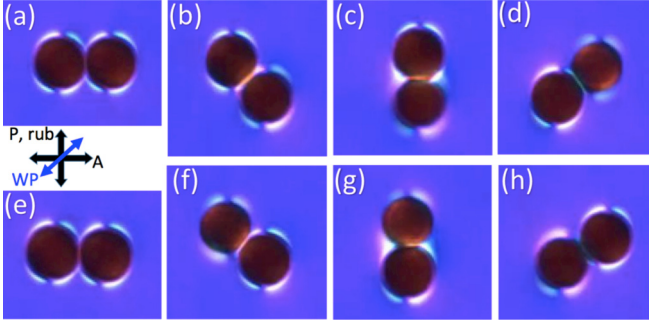
FIG. 3. (Color online) [(a)–(h)] A series of frames extracted from a video and showing rotation of a dimer of SPMBs at an elevated temperature 33.5 °C, right below the nematic-isotropic phase transition temperature of ≈35 °C. Orientations of polarizer (P), rubbing direction (rub) defining orientation of $\mathbf{n_0}$, analyzer (A), and the slow axis of a 530-nm wave plate (WP) are marked by double arrows.

surface, an important aspect in our studies. This tangential nondegenerate anchoring induces distortion of the nematic director field around the particle, creating two surface point defects called *boojums* [25–28,30–33], which are seen clearly under POM [Fig. 2(b)] at the poles of the particle along the far-field director and are schematically depicted using hemispheres in Figs. 2(c) and 2(d) for individual particles and in Figs. 2(e) and 2(f) for colloidal assemblies. In the two-dimensional director field at the interface of NLC and a single spherical SPMB, $\mathbf{n_s}$, the two boojums are singular defects that each have winding numbers +1 in $\mathbf{n_s}$, consistent with topological theorems [25], as the Euler characteristic of a spherical surface is $\chi = 2$ and the winding numbers of these two defects add to χ. In the ground state, the interparticle center-to-center separation vector $\mathbf{r_{cc}}$ is oriented at about 30° with respect to $\mathbf{n_0}$ while boojums localize at the poles of SPMBs and the boojum-to-boojum separation vector $\mathbf{r_{bb}}$ is roughly along $\mathbf{n_0}$ for each SPMB's boojum pair [Figs. 2(f) and 2(g)].

When a slowly rotating magnetic field is used to rotate individual particles and the $\mathbf{r_{cc}}$ of SPMB assemblies [Figs. 2(d) and 2(g)–2(i)] at room temperature, we observe that the two boojums tend to pin to their original locations at which they initially formed in the equilibrium $\mathbf{n(r)}$ configuration at no applied fields, so $\mathbf{r_{bb}}$ deviates from $\mathbf{n_0}$ [Fig. 2(h)]. Although the structure of director distortions in the ground state resembles that seen previously for colloidal particles with tangential degenerate anchoring, the nondegenerate (with memory) aspect of boundary conditions on our SPMBs causes pinning of $\mathbf{n(r)}$ and defects. At elevated temperatures, however, rotation of $\mathbf{r_{cc}}$ of dimers and other chainlike assemblies leaves $\mathbf{r_{bb}}$ roughly along $\mathbf{n_0}$ as the strength of pinning is strongly reduced (Fig. 3). Similar behavior is also exhibited by knot-shaped superparamegnetic microparticles [Figs. 2(j)–2(m)], which induce 12 boojums in total, 6 with positive and 6 with negative winding numbers, which is consistent with $\chi = 0$ for the trefoil torus knot surface [30]. Similarly to the case of SPMB spheres, the boojums tend to pin to their initial locations when such particles are rotated by changing the direction of a

magnetic field of 200–400 G induced by a permanent magnet (Figs. 2(j)–2(m) and Supplemental video S1 [29]).

Due to elastic interactions, colloidal microspheres with tangential surface anchoring boundary conditions for $\mathbf{n(r)}$ self-assemble into chains directed at ≈30° with respect to the far-field director [32,33], which is also the case for the studied particles [Figs. 2(e) and 2(g)]. SPMBs forming such chains cannot be controllably separated using laser tweezers. Repeated melting and quenching of the LC around particles within such chains makes them behave as single colloidal objects, with their inseparability likely aided by resin adhesion of the SPMBs in contact with each other. Each of the particles induces pairs of boojums with a total winding number +2 in $\mathbf{n_s}$ per bead [Fig. 2(e)]. At the same time, when the surfaces of particles within a chain become interconnected, the Euler characteristic of this entire object is $\chi = 2$, the same as that of an individual sphere. For N such particles with connected surfaces homeomorphic to that of a single sphere and $2N$ boojums at their poles [marked by red hemispheres for a three-particle chain in Fig. 2(e)], the total winding number in $\mathbf{n_s}$ is +2 while the winding number of $2(N - 1)$ boojums is compensated by $-2(N - 1)$ winding number of $N - 1$ neck regions between the particles [marked by blue lines in the side views of a chain shown schematically in Figs. 2(e) and 2(f)], consistent with topological theorems [25]. This is illustrated in Figs. 2(e) and 2(f) using examples of a chain of three and two colloidal microspheres forming a trimer and dimer with interconnected surfaces, respectively.

To form a colloidal SPMB dimer, we typically first let individual beads mutually attract until touching (due to elastic forces discussed above or due to a combination of elastic and magnetic forces, with the latter emerging from induced dipoles in individual beads [26]) and then melt the NLC region between particles using relatively high-power (⩾200 mW) laser traps, followed by quenching it back to the nematic phase. Surfaces of the resin particles in the ensuing dimer physically touch within a circular contact area of radius ∼0.5 µm [Figs. 2(f)–2(i) and Fig. 3]. The topology of defects induced by the dimer can be understood within a framework of the above more general discussion. The Euler characteristic of this trivially, irreversibly assembled colloidal dimer, with the surface homeomorphic to sphere, is $\chi = 2$. One would therefore expect that the net topological winding number of surface defects in $\mathbf{n_s}$ should be +2, the same as for a single sphere. Although there are typically four boojums on the two SPMBs forming a colloidal dimer [Figs. 2(f)–2(i) and Fig. 3], each having the winding number +1, topological constraints imposed by the Gaus-Bonnet and Hopf index theorems are still satisfied [25] as the neck region of the dimer has a net winding number of -2. Since the entire inter-SPMB neck region of the dimer is characterized by strong elastic distortions and, likely, also reduced order parameter [Figs. 2(g)–2(i) and Fig. 3] due to strong surface boundary conditions at the particle surfaces near the contact area, the entire vicinity of contact is essentially a spatially distributed defect of net winding number $\chi = -2$ [Figs. 2(g)–2(i) and Fig. 3]. When $\mathbf{r_{cc}}$ is aligned along $\mathbf{n_0}$, only two boojums can be identified, with the neck region and two of the original four boojums annihilating as well as mutually compensating each other and having a net winding number equal to zero [Fig. 2(i) and Figs. 3(c) and 3(g)].

By locally melting the LC around a colloidal dimer to an isotropic state, magnetically aligning $\mathbf{r}_{cc}$ in different orientations, then quenching the sample back to the nematic phase in presence of magnetic field forcing the dimer to retain this orientation with respect to confining surface rubbing direction during the quench, and, finally, turning the magnetic field off, we explored metastable states that can be obtained for such dimers due to the anchoring memory affects. We found that, in addition to the ground-state configuration with $\mathbf{r}_{cc}$ oriented along a $\sim 30°$ cone with respect to $\mathbf{n}_0$ that are similar to those formed by particles with tangentially degenerate anchoring [32,33], there are also several metastable dimer orientations, including the ones with $\mathbf{r}_{cc}$ oriented at 0 and 90° with respect to $\mathbf{n}_0$ [similarly to the ones shown in Fig. 2(i) and Figs. 3(a), 3(c), 3(e), and 3(g)]. Repeated experiments confirm that these long-lived metastable states are accessible only through melting the NLC to the isotropic state and then quenching it back to the nematic phase at room temperature. This is a natural consequence of the nondegenerate surface anchoring originating from nanoscale topography [Fig. 2(a)]. Magnetic rotations of $\mathbf{r}_{cc}$ away from stable or metastable states in the nematic phase are followed by relaxation back to these states after the field is turned off; this relaxation is driven by elastic torques originating from asymmetry of elastic distortions around the dimer during its rotation, such as in the case of the example shown in Fig. 2(h).

B. Dynamics of individual colloidal particles induced by rotating magnetic fields

The strength of applied magnetic fields (up to 108 G) is insufficient to fully and continuously rotate a single SPMB around an axis orthogonal to $\mathbf{n}_0$ when situated in a NLC host. In a magnetic field rotated at a constant rate, the sphere and $\mathbf{r}_{bb}$ rotate only up to a certain field-dependent angle α with respect to $\mathbf{n}_0$, at which magnetic and elastic torques are balanced. While the field is rotated further, $\mathbf{r}_{bb}$ is lagging until the angle between the field and $\mathbf{n}_0$ starts approaching -α, at which point the boojum-boojum axis rotates out of the plane parallel to cell substrates and circumscribes a cone of angle $\approx \alpha$ [Fig. 2(d)]. When rotating an applied magnetic field $\mathbf{H}$ in a counterclockwise (CCW) direction, as indicated by the brown arrows on the top left of Fig. 2(d), the SPMB with pinned boojums along a rotated $\mathbf{r}_{bb}$ tends to "barrel roll" out of the x-y plane, as shown by blue arrows in the inset. This barrel-roll dynamics leads to a "walking" motion of the SPMB along the x axis, which is accompanied by a precession of one of the boojums and the tilted $\mathbf{r}_{bb}$ boojum-to-boojum vector around $\mathbf{n}_0$ [boojum **2** in the right-side inset of Fig. 2(d)], while the other boojum [**1** in the right-side inset of Fig. 2(d)] usually circumscribes a smaller precessional arc. A constant net magnetic gradient force dominates the SPMB motion in the y direction [Fig. 2(d)], but motion along the x direction originates from the complex barrel-roll dynamics of the SPMB particle with the two boojums and is not present in an isotropic phase of the same NLC host. Symmetry breaking associated with this motion is assisted by the fact that gravity pulls the SPMB of density higher than that of LC closer toward the cell's bottom surface to a depth level at which particle-substrate elastic repulsion forces balance gravity. Thus, by rotational

magnetic manipulation alone one can induce SPMB translation in an NLC in a direction orthogonal to $\mathbf{n}_0$. Importantly, while the boojum-boojum axis deviates from $\mathbf{n}_0$ up to angles of $\sim 20°$ during these complex translational and rotational motions of the particle [Fig. 2(d)], the boojum defects stay pinned in roughly the same locations of the SPMB surface as they were in the static equilibrium state at no field, although their precise position can vary slightly, as we discuss in detail below.

C. Dynamics of nematic colloidal dimers in rotating magnetic fields

We studied rotating-field-induced dynamics of SPMB dimers in a 60-μm-thick, planar rubbed nematic cell infused with an LC colloidal sample that was temperature controlled between 25 °C and 33.5 °C, referred to as *room temperature* and *elevated temperature*, respectively. We applied a slowly rotating (0.01 Hz to 0.05 Hz) ac magnetic field of 108 G in the sample x-y plane. We studied the resulting dimer rotation under POM at 60 to 500 frames per second using a conventional and fast-rate cameras, respectively, as described above under Methods. For tracking positions of the surface point defects, we chose observations in a transmission-mode bright-field microscopy without polarizing optical elements [Fig. 2(d)] and also in POM where the sample is placed between two crossed polarizers, with or without an additional 530-nm phase retardation plate inserted between the sample and the second polarizer (analyzer) [Figs. 2(b), 2(g)–2(i) and 3], which provide complementary information. A detailed characterization of the ensuing rotational and translational motion of the particle dimers and accompanying defects at different conditions is summarized in Figs. 3–5.

Rotating magnetic fields allow for a full, continuous 360° rotation of $\mathbf{r}_{cc}$ of the colloidal dimer with respect to $\mathbf{n}_0$ in a plane parallel to confining substrates (Fig. 4), as well as other more complex types of rotational motion discussed below. Although the magnetic field rotation rate is slow and constant, with the field orientation angle changing linearly with time, the ensuing dynamics of particles and defects is generally complex. To quantitatively characterize these dynamics, we designated and marked the centers of particles and associated boojums, as shown in the inset of Fig. 4(a), with S1 and S2 initially being the left SPMB and the right SPMB, respectively. Each boojum was designated as B1 and B2 for the initial top and bottom boojums, respectively. Subsequent angular motions (characterized with respect to the dimer's center of mass) of these six points, corresponding to sphere centers and defects, are shown as functions of time for the $\mathbf{H}$-field rotation frequency of 0.05 Hz at room temperature [Fig. 4(a)] and at 33.5 °C [Fig. 4(b)]. Interestingly, there is a periodic structure in the rotation of the separation vector $\mathbf{r}_{cc}$ between the SPMB centers (S1, S2), which is caused by the competition between elastic and magnetic torques and is related to the so-called "flip-flop" motion (Fig. 5) of the dimer that we study below. As the SPMB dimer's orientation periodically approaches the equilibrium low-energy state and departs from it during the periodic motion, the elastic torque decreases and increases in strength, respectively. This causes the respective modulation of angular velocity exhibited by $\mathbf{r}_{cc}$ of the dimer during rotation [Fig. 4(a)]. In this way, a dimer
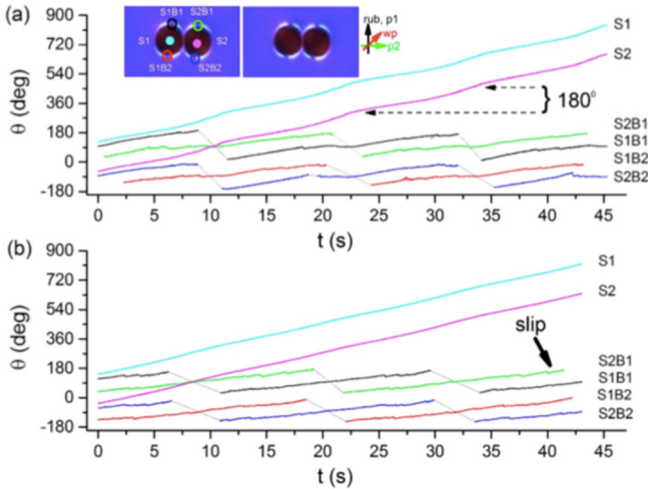
FIG. 4. (Color online) SPMB and boojum angular motion with respect to the SPMB dimer center of mass at two different temperatures. A magnetic field is rotated at a slow, constant rate of 0.05 Hz clockwise in the x-y plane, thus rotating a SPMB dimer at the same average rate. Dynamics of SPMBs and boojums is characterized in terms of azimuthal angles θ describing azimuthal orientations of the corresponding separation vectors connecting the dimer's center of mass with these particle centers and boojums, respectively. (a) Colloidal particle and boojum motion at a room temperature. The inset shows a configuration of a SPMB dimer with each SPMB center of mass and each boojum on the polarizing optical micrograph designated as follows for the initial configuration shown in the inset: Left SPMB (S1), right SPMB (S2); each boojum is assigned to its SPMB. For example, S2B2 is the right SPMB, second boojum (lower right boojum). The second POM micrograph without markings shows details of how boojums of each particle position themselves on the microsphere. All colloidal particle and boojum rotational motion versus time are probed with respect to the dimer center of mass as the reference frame; the time dependencies describing rotational motions of defects and particles are labeled at the right side of the plot. Orientations of crossed polarizers (p1 and p2), rubbing direction (rub) defining orientation of $\mathbf{n_0}$, and the slow axis of a 530-nm wave plate (wp) are marked by arrows. The thin lines interrupting the dependencies in graphs correspond to the time intervals of rotation when the boojums cannot be localized within the neck regions. (b) Similar colloidal particle and boojum dynamics at an elevated temperature of 33.5 °C, with the arrow indicating slip motion of one of the surface defects.

FIG. 5. (Color online) SPMB dimer rotation and the ensuing "flip-flop" dynamics under the rotating magnetic field. [(a)–(g)] Optical micrographs showing the dimer as viewed in the lateral x-y plane with the rubbing direction along y. Shown above each frame is a reference schematics depicting the dimer tilt out of the x-y plane, along with the "flip-flop" indication. The colored (gray) dots distinguish centers of the two SPMBs; the SPMB's split coloring [white and brown (dark gray)] distinguishes the top and bottom hemispheres of the dimer, respectively. (h) Details of the dimer "flip-flop" motion showing a +180° "flip" within its first 180° in-plane rotation, followed by a -180° "flop" during its second 180° in-plane rotation. The coloring of the halves of spheres in the schematics provides insights into the complex rotations of dimers, as seen from different view directions along the axis shown in (a)–(h).

undergoing magnetic rotation "lags" the applied field **H** every 180° of rotation, giving rise to the corresponding periodic pattern in this behavior. Since the Reynolds and Ericksen numbers associated with the studied particle motions in the NLC are small, the inertia effects and coupling of rotation-induced flow with the director field can be neglected. Thus, the points of the slowest dimer rotation [Fig. 4(a)] roughly correspond to highest elastic free energy of distortion (and the rotation-opposing elastic torque) and are observed when the dimer's $\mathbf{r_{cc}}$ is rotated far from its equilibrium orientation with respect to $\mathbf{n_0}$. This modulation becomes considerably weaker at elevated temperatures [Fig. 4(b)], which is related to the corresponding decreased values of elastic constants and thus also the elastic torque scaling linearly with these constants.
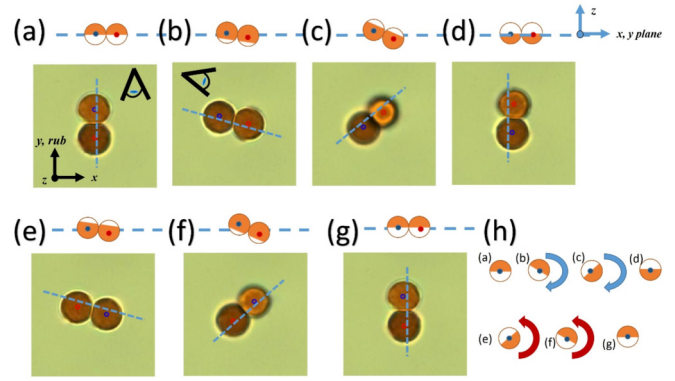
In addition, anchoring memory effects are also weaker at elevated temperatures. Since gravity pulls a dimer below the nematic cell midplane to a levitation depth level at which it is balanced by repulsive SPMB-substrate elastic forces [28], different forms of dimer rotations can also be accompanied by slow translational motion, similarly to that of individual spheres [Fig. 2(d)].

As the strength of the magnetic field is lowered (e.g., to ∼80 G) so that $\mathbf{r_{cc}}$ fails fully following the magnetic field rotation, we note that the same colloidal pair that was continuously rotating at 108 G starts to "flip" +180° (Fig. 5). This is prompted by the dimer's rotation lagging the rotation of the magnetic field corresponding to a reduction of the total elastic and magnetic free energy when the dimer escapes the x-y plane and rotates on an "escape" cone to a lower-energy orientational state (Fig. 5), similarly to what we discussed for individual spheres above. This "flip" out of the plane parallel to substrates occurs during the first 180° of the magnetic field rotation and is completely reversible via the so-called "flop" motion, a similar but opposite -180° rotation during the second 180° in plane rotation of the field [Fig. 5(h)]. This complete cycle of "flip-flop" motion happens once during every 360° in-plane rotation of the field, with each flip and flop happening due to the "lag" of the dimer's rotation with respect to **H**. We note that this "lagging" (at the same applied magnetic field strength) is reduced when the sample temperature is elevated significantly above room temperature [Fig. 4(b)] and in fact disappears completely as the NLC transitions to an isotropic phase at ≈35 °C. This is natural as the NLC elastic structure's effect on colloid motion is removed when the LC transforms into an isotropic liquid. Because of
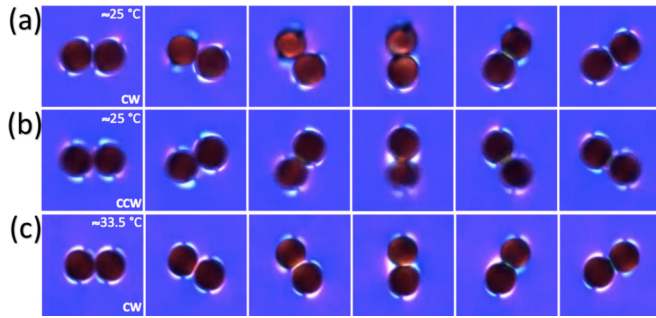
FIG. 6. (Color online) POM micrographs showing details of SPMB dimer rotation [(a) and (b)] with and (c) without "flip-flop" dynamics under magnetic field **H** rotated in the [(a) and (c)] CW and (b) CCW directions.
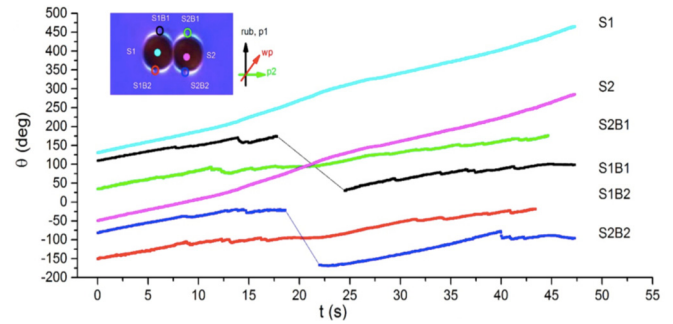

FIG. 7. (Color online) SPMB and boojum angular motion with respect to the SPMB dimer's center of mass at room temperature characterized in terms of azimuthal angles θ describing azimuthal orientations of the corresponding separation vectors connecting the dimer's center of mass with these particle centers and boojums, respectively. A magnetic field is rotated at a constant rate of 0.02 Hz clockwise in the x-y plane, thus rotating the SPMB dimer. The inset shows a configuration of the SPMB dimer with each SPMB center of mass and each boojum designated as follows: Left SPMB center (S1), right SPMB center (S2), and each boojum assigned to its SPMB. For example, S2B1 is the right SPMB, second boojum (lower right boojum). The figure shows all particle and boojum rotational motions versus time using the dimer center of mass as the reference frame; the experimental curves are labeled on the right side of the plot. Sharp jumps in the angle versus time curves indicate the "boojum slipping." The thin lines interrupting the dependencies in graphs correspond to the time intervals of rotation when the boojums cannot be localized within the neck regions.

the gravity-induced asymmetry discussed above, the dimer flip-flop motion manifests itself somewhat differently for clockwise (CW) and CCW field rotations [Figs. 6(a) and 6(b)] because it is associated with the $\mathbf{r}_{cc}$ moving out of the initial lateral plane parallel to substrates (manifested by the SPMB beads going out of focus in the corresponding POM images). At an elevated temperature of $\approx 33.5\,°\mathrm{C}$, however, $\mathbf{r}_{cc}$ closely mimics rotation of **H** while staying parallel to cell substrates [Fig. 6(c)]. Assemblies with three and more particles exhibit qualitatively similar behavior when self-organized into straight chains and different dynamics when their chains are not straight. Due to a large number of possible assemblies and the ensuing types of dynamics for three and more particles, we restrict our experimental exploration in this work to individual SPMBs and their dimers.

D. Stick-slip dynamics of boojums on rotating colloidal microspheres

Interestingly, magnetic rotation of a dimer pair leads to an unexpected "sticking and slipping" of boojums along the surfaces of colloidal particles. This behavior presents itself as a series of jumps in the angular positions of the boojums with respect to the dimer's center of mass. An example of a "boojum slip" is indicated in Fig. 4(b), but smaller slips are not obvious in most cases due to representing relatively small jumplike angular changes as compared to the large overall angular rotation that in this Fig. 4 demonstrates periodicity in lagging of dimer's dynamics relative to **H** during the repeated rotation. To quantify these fascinating dynamics, we probed details of boojum motions at two temperatures, 25° and 33.5 °C, and at three different rotational frequencies (0.01, 0.02, and 0.05 Hz), all in the counterclockwise rotational direction and at the rotating field strength of 108 G. Representative motions at 0.02 Hz are shown in Figs. 7 and 8 for data taken at 25 ° and 33.5 °C, respectively, with each SPMB and boojum designated as discussed above.

Within the used range of rotation rates and temperatures, rotation at 0.02 Hz produces the clearest "stick-slip" motion of a boojum along the SPMB surface (Fig. 7). We note that temperature plays a crucial role in determining not only the frequency of slip occurrences but also the slip amplitude. At 25 °C the slips occur infrequently, have large amplitudes of approximately 5°–20° (Fig. 8) and tend to occur

FIG. 8. (Color online) SPMB and boojum angular motions with respect to the dimer's center of mass at an elevated temperature of 33.5 °C. A magnetic field is rotated at a constant rate of 0.02 Hz clockwise in the x-y plane, thus rotating the SPMB dimer, causing the boojum motion. The inset shows a configuration of the dimer with each SPMB center of mass and each boojum designated as follows: Left SPMB (S1), right SPMB (S2), and each boojum assigned to its SPMB. For example, S2B1 is the top right boojum on the surface of the right SPMB. The figure shows rotation of separation vectors connecting the SPMB dimer's center-of-mass reference frame and the particle centers of mass and boojums described using angle versus time (labeled on the right side of the plot). Boojum slipping is apparent. Sharp angular jumps are "boojum slips." The thin lines interrupting the dependencies in graphs correspond to the time intervals of rotation when the boojums cannot be localized within the neck regions.
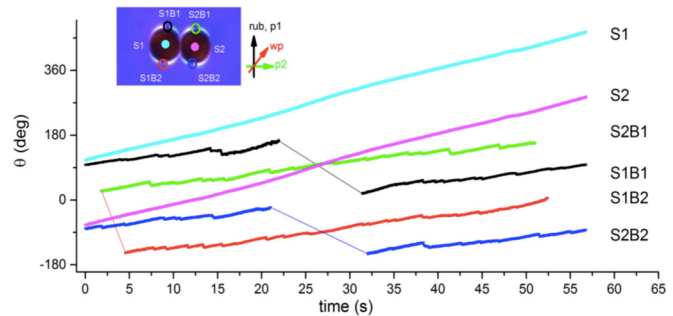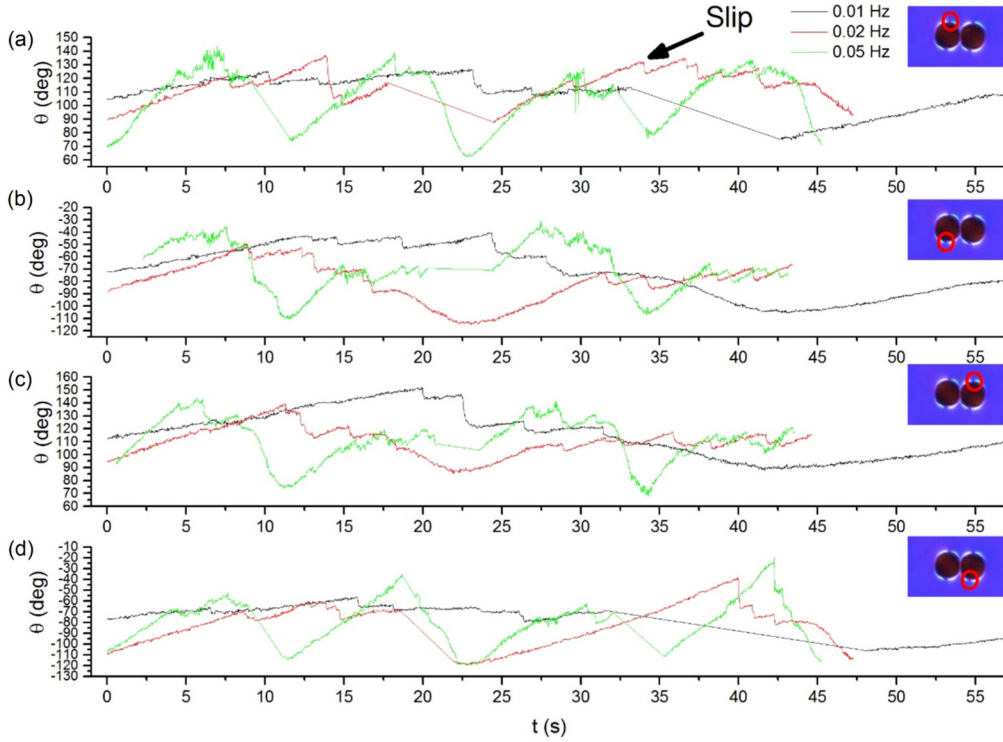
FIG. 9. (Color online) Boojum angular motion with respect to the corresponding SPMB's center of mass at room temperature. Inset image in (a)–(d) indicates the SPMBs boojum that is tracked for a total of four plots. Each line indicates a different angular frequency of magnetic field and dimer rotations: 0.01 Hz (black), 0.02 Hz [red (dark gray)], and 0.05 Hz [green (light gray)]. Note that boojum slipping frequency and amplitude are both dependent on the rotation rate. A representative instance of boojum stick-slip is called out with a black arrow in (a). The thin lines interrupting the dependencies in graphs correspond to the time intervals of rotation when the boojums cannot be localized within the neck regions.

at boojum's $\mathbf{r_{bb}}$ deflection to $\sim\pm30°$ from $\mathbf{n_0}$. This makes sense from the standpoint of elastic distortion of the local director field. As the dimer rotates, elastic free energy of the surrounding structure increases due to elastic deformation of the director. Surface anchoring and easy axis pinning on the SPMB surface withstand this elastic distortion to a point, at which the system is forced to reminimize its elastic and surface anchoring free energy through relocating the boojums, changing $\mathbf{n_s}$ at the particle surface, and partially removing the $\mathbf{n(r)}$ distortions. This can occur through several dynamic pathways, such as the so-called "flip-flop" motion described previously in Fig. 7 or through slipping of the pinned surface anchoring conditions associated with locations of the boojums or through combinations of the two. This anchoring-mediated resistance to slipping can be thought of in terms of a potential barrier landscape, with the nondegenerate surface anchoring determining the potential barrier landscape responsible for the stick-slip motion.

E. Effects of temperature

When the temperature of the sample is elevated to 33.5 °C, which is $\sim$2°C below the nematic-isotropic transition temperature, we note that the frequency of slips increases significantly [Figs. 9 and 10] while the amplitude is commensurately reduced. High-temperature slips tend to start occurring at angles of around $\pm95°$–100°, which corresponds to $\mathbf{r_{cc}}$ deviated to $\pm5°$–10° away from the far-field director. Again, this makes sense from the standpoint of view of the potential

barrier landscape model described above. Since the slipping process is determined by the strength of surface pinning, an elevation in temperature lowers the energetic barrier in terms of corresponding elastic and surface anchoring energies resisting this motion. By plotting angular motion versus time for all studied boojums at room temperature and at 33.5 °C as well as at frequencies ranging from 0.01 to 0.05 Hz, we can comparatively characterize the key features of the boojum's stick-slip motion at these different experimental conditions (Figs. 9 and 10).

Interestingly, as the temperature of the NLC is elevated closer to its nematic-isotropic transition temperature, the "flip-flop" dynamics of the dimer practically disappears. The dimer flip-flops happen due to this motion being the most efficient pathway to minimize the elastic and surface anchoring free energy of the local distorted director field as the particles are slowly rotated and the elastic and magnetic torques compete with each other. However, as the temperature of the NLC is increased, boojum slipping becomes more likely and frequent, and thus the observed rearrangement of defects becomes a competing dynamic pathway to minimize the elastic free energy of deformation under these conditions. Mutual dynamics of defects and colloidal particles in this case is complex and difficult to study as the defect motion trajectories are three dimensional in nature and localization of defects is complicated by their interaction with the neck region of the dimer director configuration. However, as experimental parameters such as temperature and field and anchoring
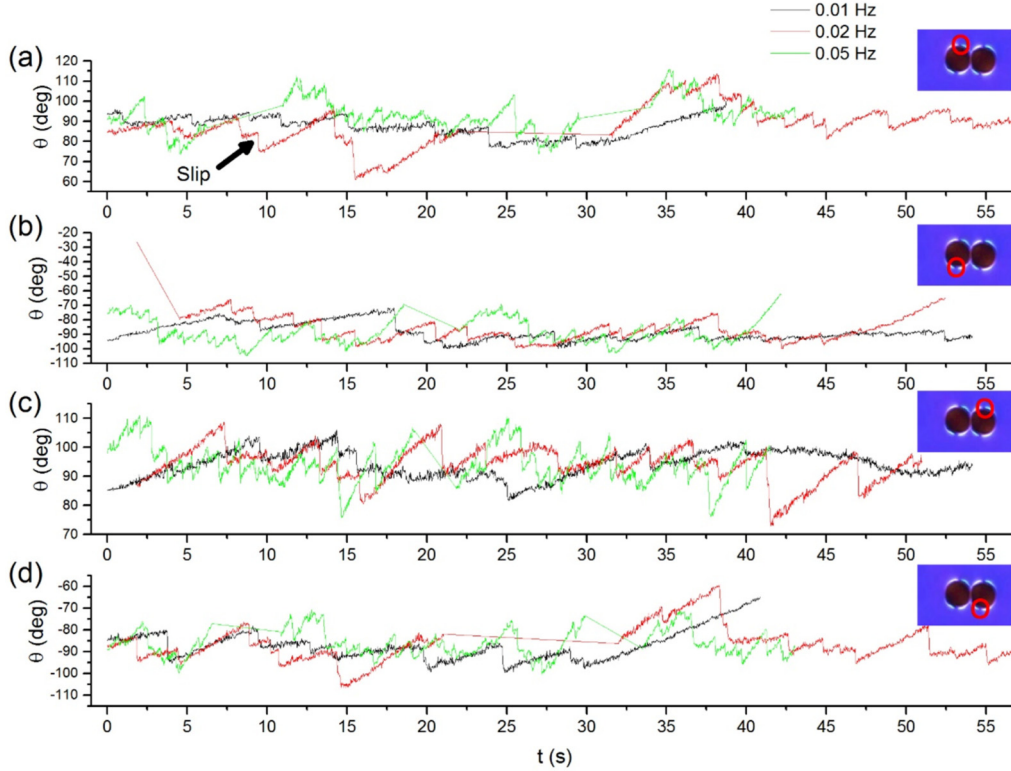
FIG. 10. (Color online) Boojum angular motion with respect to its SPMB's center of mass at an elevated temperature of 33.5 °C. The inset image in (a)–(d) indicates the tracked boojums on a colloidal dimer for a total of four plots. Each line corresponds to a different angular frequency of dimer rotation: 0.01 Hz (black), 0.02 Hz [red (dark gray)], and 0.05 Hz [green (light gray)]. The comparison of these data shows that boojum slipping period and amplitude are dependent on the rotation rate and temperature. A representative instance of boojum stick-slip is called out with a black arrow in (a).

strengths are varied, one can distinguish three different regimes: (1) "flip-flop" motion of colloidal dimers with strong sticking of boojums to SPMB surfaces; (2) continuous rotation of dimers with stick-free slipping of boojums; (3) a combination of the above two regimes, which is the most common, with the continuous dimer rotation accompanied by different types of "flip-flop" dynamics of particles and "stick-slip" dynamics of boojums. The Supplemental videos S2 and S3 [29] show how these different types of motion manifest themselves at room and elevated temperatures of the NLC sample, respectively.

F. Time-resolved kinetics of boojum slipping

To accurately quantify the details of the dynamics of individual boojum slip events, we used a high-speed camera operating at >500 fps (Fig. 11). This allowed us to obtain enough frames and the corresponding boojum position data points (extracted from video-microscopy-based position tracking) to quantitatively characterize the fast kinetics of individual surface defect slips at an elevated temperature of 33.5 °C. We observe a generally sigmoidal behavior of the slip [Fig. 11(a)], with the boojum's angular position versus time described by

$$\theta(t) = \theta_0 \frac{1}{1 + e^{-t/\tau}}, \tag{3}$$

where τ is a characteristic time constant and θ_0 is the initial angular position prior to the slip. A sigmoidal response is

an identifying characteristic of stick-slip behavior in different physical systems [6–7]. Fitting of experimental data using Eq. (3) benefits from subtracting the steady-state change in angle with respect to time from the experimentally measured response data [Fig. 11(b)], allowing us to better quantify the slip motion. A boojum slip [Fig. 11(a)] in this instance is characterized by a jumplike angular motion with an amplitude of approximately 15° with respect to the far-field director and a sigmoidal-like profile [with the sigmoidal fit shown by a blue line in Fig. 11(a)]. Fitting the raw experimental data yields a characteristic slipping time constant $\tau_s \sim 0.0036$ s [Fig. 11(a)]. By compensating for the background constant-rate change of the angle versus time due to sticking of the boojum to the rotating SPMB [Fig. 11(b)], we obtain a sigmoidal (red line) fit yielding $\tau_s \sim 0.0034$ s. Note that the exponential fit (green line) does not represent a fit over the entire dynamical process, unlike the sigmoidal fit [Fig. 11(b)]. This finding further confirms that the dynamics of surface defects in our experiments is a stick-slip motion as the sigmoidal time dependence is a salient feature of stick-slip dynamics in diverse physical systems [1–5].

IV. DISCUSSION

Figure 12 shows dynamics of boojums presented in the form of spatial displacements of these defects on SPMB surfaces as a function of the angle φ of rotation of $\mathbf{r_{cc}}$ of a dimer of SPMB particles accompanied by these defects. These results
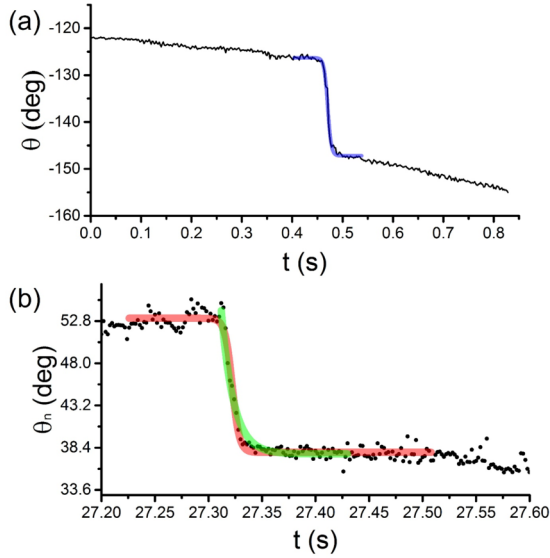
FIG. 11. (Color online) Detailed analysis of a representative single boojum "slip" event using a high-speed camera operating at 500 fps. (a) Boojum's angular position change θ versus time due slipping motion with respect to the dimer's center of mass, with a sigmoidal fit [blue (gray) line] yielding the time constant $\tau_s \sim 0.0036$ s (fitting with $R^2 = 0.995$). (b) Boojum angular slipping motion θ_n with respect to the colloidal dimer's center of mass after the constant change of angle with respect to time subtracted and exhibiting a sigmoidal [red (dark gray) line] fit of $\tau_s \sim 0.0034$ s (fitting with $R^2 = 0.987$) and exponential [green (light gray) line] $\tau_e \sim 0.0012$ s (fitting with $R^2 = 0.946$).

reveal that there is no well-defined correlation between the slipping of individual boojums on SPMB surfaces, which is a natural finding as the system is highly overdamped even at the

fastest implemented SPMB dimer rotation rates. Slipping of individual boojums is accompanied by local rearrangements of $\mathbf{n}(\mathbf{r})$ in the proximity of the microsphere around the boojum undergoing a slip. The typical distance amplitude of a slip is ~ 1 μm (Fig. 12). This distance between the locations of a boojum on the surface of a microsphere before and after the slip is much larger than the length scale of nanoscale roughness of SPMB's surface topography [Fig. 2(a)] but smaller than the perimeter of a circular trajectory on which it moves during rotation. As a SPMB colloidal particle is rotated, the free-energy cost of elastic distortions overcomes the strength of coupling due to nondegenerate surface anchoring, while kinetics of boojum slipping processes on surfaces of rotating SPMBs are determined by the competition between elastic and viscous torques. The former arises due to memorized nondegenerate planar boundary conditions at particle surfaces of diameter $2R = 4.5$ μm. We can therefore roughly estimate the characteristic time of boojum slipping (Fig. 11) as the director relaxation time corresponding to relaxation of the director on the length scale comparable to the particle size: $\tau_{slip} \propto \gamma_1 R^2/(\pi^2 K)$ [14], where $\gamma_1 \approx 0.08$ Pa s is the rotational viscosity and $K = 7$ pN is an average elastic constant of the used LC, similarly to estimates of the director relaxation times due elastic distortions of other origins [14]. This yields an estimate of $\tau_{slip} = 1-10$ ms, consistent with the experiments (Fig. 11). The kinetics of the individual slip events (Fig. 11) resembles that of analogous phenomena occurring in very different physical systems [2–5,34]. For example, sigmoidal-like dependencies of position versus time similarly to the ones shown in Fig. 11 are characteristic for the so-called silent earthquakes [34].

The core structure of boojums was recently shown to be split into semirings of small singular half-integer disclinations [25,28,35], but only smooth spherical surfaces have
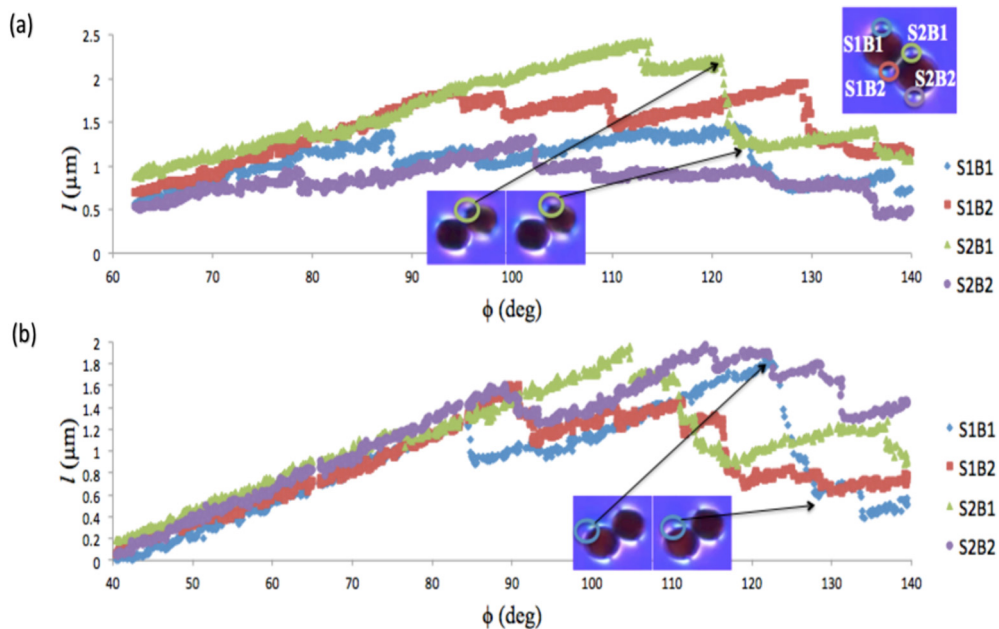

FIG. 12. (Color online) Displacement of boojums l along the SPMB surface as a function of the angle ϕ between $\mathbf{r_{cc}}$ and $\mathbf{n_0}$ at (a) 0.01 Hz and (b) 0.02 Hz rotation rates of magnetic field. The top-right inset in (a) shows labeling of boojums on the two spheres of a colloidal dimer. The bottom insets depict changes of positions of encircled boojums as a result of slip events indicated by arrows.

been considered so far. It will be of great fundamental interest to explore how the nonuniform nanostructured surface morphology of colloidal beads like our SPMBs can alter this behavior, potentially making it rather complex as the characteristic size of surface features of SPMBs is comparable to or larger than the nematic coherence length [Fig. 1(a)] [35]. Even more interesting questions posed by our work include the problem of kinetics of such boojums with split cores during stick-slip motion. Beyond random topographic patterns studied here, nanostructured surface topography of particles can be potentially designed to favor different types of alignment of colloidal particles in LCs, differing from what can be expected for colloidal objects with nanoscale-smooth surfaces and homogeneous boundary conditions, which may be of practical importance for applications in photonics and electro-optics. Since the boojum pinning is observed not only in the case of spherical SPMBs but also for complex-shaped colloidal particles such as trefoil knots (Fig. 2), this opens the possibility of experimental exploration of the role of surface topology in determining the stick-slip dynamics of surface point defects.

The effects of host fluid confinement are known to enrich the dynamics of suspended magnetically controlled colloidal particles, such as anisotropic colloidal doublets [36]. However, the effective symmetry breaking due to defects, nematic elasticity, and low-symmetry director distortions at applied rotating magnetic fields and their coupling to the effect of nearby confining substrates enrich this behavior even further [Fig. 2(d)], so even single spherical colloidal particles can exhibit complex translational and rotational motion in a rotating magnetic field, which differs from the behavior of similar colloidal particles in isotropic fluid hosts, as tested by heating the LC to the isotropic phase. Since this complex magnetically controlled dynamics of individual SPMBs and their assemblies is dependent on the orientation of the director in the surrounding LC, which can be controlled by optically defining surface boundary conditions on confining glass substrates [37], this finding opens the possibility of programmed, reconfigurable guiding of colloidal swimmers directed by a combination of rotating magnetic fields and low-intensity light [37], which will be the focus of our future studies.

V. CONCLUSIONS

We have observed and characterized the stick-slip motion of surface point defects along colloidal particle surfaces in uniformly aligned nematic liquid crystals when these colloidal particles are manipulated by rotating magnetic fields, as well as demonstrated the rich rotational and translational dynamics of these magnetically responsive colloids themselves. This complex motion is shown as being prompted by a competition between nondegenerate surface anchoring "with memory" and elastic and magnetic torques rotating superparamagnetic colloidal spheres. In particular, analysis of the stick-slip motion revealed a sigmoidal-type response of angular positions of boojums versus time, indicative of the stick-slip behavior. We also described unusual translational dynamics of spherical superparamagnetic particles induced by rotating magnetic fields, showing that these occur as a result of their rotational motion and elastic coupling to the director field of the surrounding LC, as they differ from the behavior of magnetically controlled colloidal particles dispersed in isotropic fluids [36]. Our findings expand the scope of nonequilibrium phenomena in liquid crystal colloids and may lead to new insights into dynamics of surface-bound defects as well as practical applications in designing and construction of nano- and micromachines utilizing the interplay between dynamics of magnetically controlled colloidal particles and defects. The observed dynamics of defects enriches the known types of stick-slip motion in soft matter systems [21,38–45] and may enable their uses as model systems for quantitative studies of these types of nonequilibrium behavior.

[1] Z. Deng, A. Smolyanitsky, Q. Li, X. Feng, and R. J. Cannara, Nat. Mater. **11**, 1032 (2012).

[2] H. L. Kuntz and R. D. Bruce, J. Acoust. Soc. Am. **77**, S4 (1985).

[3] W. F. Brace and J. D. Byerlee, Science **153**, 990 (1966).

[4] S. N. Patek and J. E. Baio, J. Exp. Biol. **210**, 3538 (2007).

[5] N. H. Fletcher and T. D. Rossing, *The Physics of Musical Instruments*, 2nd ed. (Springer, Berlin, 2005).

[6] J. P. Hirth and J. Lothe, *Theory of Dislocations* (Wiley, New York, 1982).

[7] A. Guran, F. Pfeiffer, and K. Popp, *Dynamics with Friction: Modeling, Analysis and Experiment* (World Scientific, Singapore, 1996).

[8] J. O. Marston, P. W. Riker, and S. T. Thoroddsen, Sci. Rep. **4**, 4326 (2014).

[9] J. Frieldel, *Dislocations* (Pergamon Press, New York, 1964).

[10] A. Vilenkin and E. P. S. Shellard, *Cosmic Strings and Other Topological defects* (Cambridge University Press, Cambridge, 1994).

[11] T. W. B. Kibble, J. Phys. A **9**, 1387 (1976).

[12] W. H. Zurek, Nature **317**, 505 (1985).

[13] I. Chuang, B. Yurke, A. N. Pargellis, and N. Turok, Phys. Rev. E **47**, 3343 (1993).

[14] P. G. de Gennes and J. Prost, *The Physics of Liquid Crystals* (Clarendon Press, Oxford, 1993).

[15] M. Kleman, *Points, Lines and Walls in Liquid Crystals, Magnetic Systems and Various Ordered Media* (Wiley, Chichester, 1983).

[16] I. I. Smalyukh and O. D. Lavrentovich, Phys. Rev. Lett. **90**, 085503 (2003).

[17] I. I. Smalyukh and O. D. Lavrentovich, Phys. Rev. E **66**, 051703 (2002).

[18] R. Holyst and P. Oswald, Int. J. Mod. Phys. B **09**, 1515 (1995).

[19] M. Gu, I. I. Smalyukh, and O. D. Lavrentovich, Appl. Phys. Lett. **88**, 061110 (2006).

[20] S. Lemerle, J. Ferre, C. Chappert, V. Mathet, T. Giamarchi, and P. Le Doussal, Phys. Rev. Lett. **80**, 849 (1998).

[21] C. Blanc, M. Nespoulous, E. Angot, and M. Nobili, Phys. Rev. Lett. **105**, 127801 (2010).

[22] A. I. Larkin and Yu. N. Ovchinikov, J. Low Temp. Phys. **34**, 409 (1979).

[23] N. D. Mermin, Phys Today **34**(4), 46 (1981).

[24] N. D. Mermin, *Boojums All the Way Through: Communicating Science in a Prosaic Age* (Cambridge University Press, Cambridge, UK, 1990).

[25] Q. Liu, B. Senyuk, M. Tasinkevych, and I. I. Smalyukh, Proc. Natl. Acad. Sci. USA **110**, 9231 (2013).

[26] M. C. M. Varney, N. J. Jenness, and I. I. Smalyukh, Phys. Rev. E **89**, 022505 (2014).

[27] P. M. Chaikin and T. C. Lubensky, *Principles of Condensed Matter Physics* (Cambridge University Press, Cambridge, 1995).

[28] M. C. M. Varney, Q. Zhang, M. Tasinkevych, N. M. Silvestre, K. A. Bertness, and I. I. Smalyukh, Phys. Rev. E **90**, 062502 (2014).

[29] See Supplemental Material at http://link.aps.org/supplemental/10.1103/PhysRevE.91.052503 for movies of magnetic rotation of spherical and knot-shaped magnetically responsive particles.

[30] A. Martinez, M. Ravnik, B. Lucero, R. Visvanathan, S. Žumer, and I. I. Smalyukh, Nat. Mater. **13**, 258 (2014).

[31] B. Senyuk, M. C. M. Varney, J. A. Lopez, S. Wang, N. Wu, and I. I. Smalyukh, Soft Matter **10**, 6014 (2014).

[32] P. Poulin and D. A. Weitz, Phys. Rev. E **57**, 626 (1998).

[33] I. I. Smalyukh, O. D. Lavrentovich, A. N. Kuzmin, A. V. Kachynski, and P. N. Prasad, Phys. Rev. Lett. **95**, 157801 (2005).

[34] S. I. Franco, V. Kostoglodov, K. M. Larson, V. C. Manea, M. Manea, and J. A. Santiago, Earth Planets Space **57**, 973 (2005).

[35] M. Tasinkevych, N. M. Silvestre, and M. M. Telo da Gama, New J. Phys. **14**, 073030 (2012).

[36] P. Tierno, R. Golestanian, I. Pagonabarraga, and F. Sagues, Phys. Rev. Lett. **101**, 218304 (2008).

[37] A. Martinez, H. C. Mireles, and I. I. Smalyukh, Proc. Natl. Acad. Sci. USA **108**, 20891 (2011).

[38] M. A. Ray, H. Kim, and L. Jia, Langmuir **21**, 4786 (2005).

[39] H. Bodiguel, F. Doumenc, and B. Guerrier, Langmuir **26**, 10758 (2010).

[40] J. Hasnain, S. Jungblut, and C. Dellago, Soft Matter **9**, 5867 (2013).

[41] A. Askounis, K. Sefiane, V. Koutsos, and M. E. R. Shanahan, Phys. Rev. E **87**, 012301 (2013).

[42] M. Griffa, B. Ferdowsi, R. A. Guyer, E. G. Daub, P. A. Johnson, C. Marone, and J. Carmeliet, Phys. Rev. E **87**, 012205 (2013).

[43] V. L. Morales, J.-Y. Parlange, M. Wu *et al.*, Langmuir **29**, 1831 (2013).

[44] T. Troy, N. H. Kim, and N. N. Thyagu, Proc. Natl. Acad. Sci. USA **109**, 10806 (2012).

[45] A. Eremin, C. Bohley, and R. Stannarius, Phys. Rev. E **74**, 040701 (2006).